THE PREDICTION OF SEPARATED FLOW USING A VISCOUS-INVISCID INTERACTION METHOD

ICAS-84-2.3.3

B. R. Williams
Royal Aircraft Establishment
Farnborough, Hampshire

Abstract

The separation of boundary-layer flow from a wing or in a diffuser usually defines the limit of efficient operation, so it is important that the onset and development of separated flow can be predicted. The calculation of the interaction of the shear layer close to the aerofoil with the external inviscid flow has offered an attractive alternative to solving the Reynolds-averaged Navier Stokes equations for attached flow: the interaction method is much faster. In this paper it is shown how the interaction approach can be extended for use with separated flows and the development of a practical method is described. The calculation of the shear layer through the singularity at separation is accomplished by using an inverse mode. Beyond separation the empirical definition of a new family of velocity profiles allows an integral calculation of the shear layer to proceed up to the reattachment. The solutions for the shear layer close to the aerofoil are matched to the external inviscid flow by a 'semi-inverse' method[1]. A careful examination of the stability of this method leads to rapid convergence for separated and attached flows. As an illustration the stall and post stall behaviour of a two-dimensional aerofoil is predicted and compared with experimental results.

I. Introduction

A limiting factor in the performance of an aerofoil is defined by the stall at which the flow separates from the upper surfaceof the aerofoil and the lift force usually decreases with an increase in the angle of incidence. An aerofoil designer would like to be able to predict with confidence the angle of incidence at which the stall occurs and the lift and drag coefficients at and beyond the stall, ie he would like to be able to calculate the viscous effects for both attached and separated flow. A recent survey[1] has indicated that for attached flows on aerofoils the effects of viscosity can be estimated by matching a calculation of the outer inviscid flow with a calculation of the development of the boundary layer close to the surface of the aerofoil. However there appeared to be several obstacles preventing the extension of this technique to separated flows.

The first obstacle occurs at the separation point, for an integration of the boundary-layer equations with a specified pressure distribution will encounter the singularity at the point of separation and the calculation is unable to proceed any further. Catherall and Mangler[2] first demonstrated for laminar boundary layers that the singularity is not present if the boundary layer equations are integrated in 'inverse mode' for which the displacement surface is specified and the pressure distribution is calculated. East et al[3] used a development of Green's[4] lag-entrainment method and produced an integral formulation of an inverse method for tubulent boundary layers.

The second obstacle is the integration of the boundary-layer equations through the separated region in which the velocity profile has reversed flow. Le Balleur[5] and Lock[6] have developed two-parameter velocity-profile families which can be used to describe both attached and separated flows. The inclusion of these velocity profiles into the integral boundary-layer method can give satisfactory predictions of the separated flow over the surface of the aerofoil close to the trailing edge.

The third obstacle is concerned with the matching of the outer inviscid flow and a separated boundary layer which no longer obeys the classical boundary-layer approximations. This difficulty is overcome by replacing the equations describing the shear layer by some higher order approximation to the Navier-Stokes equations than the boundary-layer equations. There are two popular methods for matching the outer inviscid flow with the shear layer. In the first, originally described by Bradshaw and Mahgoub[7], the flows are matched along some arbitrary line, in the essentially inviscid flow, which encloses the aerofoil and its associated shear layers. This approach is more suited to finite-difference solutions of the shear-layer equations. In the second method the inviscid flow is extended through the shear layer to the surface of the aerofoil and to a convenient line in the wake dividing the flows from the upper and lower surfaces of the aerofoil by the 'deficit formulation' as described by East[8] and Le Balleur[5]. This approach is suited to integral solutions of the shear layer.

The fourth obstacle is concerned with obtaining convergence in the matching of the outer inviscid flow with the inner shear layer. For a 'direct scheme', in which the aerofoil shape, with modified surface boundary conditions, is specified for the inviscid scheme and the resulting pressure is used for the shear-layer calculation, practical experience has shown that severe under-relaxation is required to obtain convergence as the flow approaches separation. The relaxation factor is obtained by numerical experiments and cannot automatically be transferred to new calculations. As mentioned above the shear-layer calculation in direct mode cannot proceed past the point of separation so that it is necessary to calculate the shear length in inverse mode. The inverse shear-layer calculation can be matched either with an inverse inviscid calculation (ie the pressure is specified and the shape calculated) to give a 'fully inverse' scheme or with a direct inviscid calculation to give a 'semi-inverse' scheme. Following Le Balleur[5] and Wigton and Holt[9] the stability of these schemes is analysed by a Fourier analysis. It is found that the direct scheme is

stable and can be made to converge for attached flows but in general is unstable for separated flows. The fully inverse method is stable for separated flows but the relaxation factor is inversely proportional to the size of the computational domain which results in slow convergence for external aerodynamics where a large but finite computing domain is used. The semi-inverse scheme is stable for attached and separated flows and the Fourier analysis gives optimum values for the relaxation factor. The relaxation factors takes different values at points on the aerofoil and depends upon the state of the boundary layer and the discretisation of the aerofoil in the inviscid method.

The method of overcoming these difficulties is illustrated by the calculation of the incompressible flow about a two-dimensional aerofoil upto and beyond the stall. The restriction to incompressible flow gives a linear problem for the outer inviscid flow and allows a surface singularity method to be used: this is described in section III. The inclusion of second order terms in the integral formulation of the shear-layer equations and their solution in inverse mode is described in section IV. The section also describes the insertion of the two-parameter velocity-profile family into the shear-layer method. The 'semi-inverse' method is described in section V and the results of the stability analysis for all three schemes are given. In section VI the flow about a NACA 4412 aerofoil is calculated up to and beyond the stall and the results are compared with experimental measurements taken recently at RAE[10] and with the measurements of Wadcock[11].

II. Boundary Conditions for the Outer Inviscid Flow

The calculation of flows with separation should include the effects of higher order terms in the matching of the outer inviscid and shear-layer flows and in the calculation of the development of the shear layer. The matching of the flows including an approximation of second order terms has been described in detail by Lock and Firmin[1] and only a summary of the relevant points is given here.

It is assumed that the flow field can be split into two regions; an inner region described by the Navier-Stokes equations (or some approximation of these equations) and an outer region described by the Euler equations, which for irrotational, incompressible flow are approximated by Laplace's equation. If an integral formulation is used for the shear layer then the most attractive model for the displacement effect of the shear layer is to apply transpiration at the boundary surface. For this model the definition of the inviscid flow must be extended from the outer edge of the shear layer onto the surface of the aerofoil and a convenient line in the wake dividing the flows from the upper and lower surfaces of the aerofoil. Following Lock and Firmin[1] the new inviscid flow is called the equivalent inviscid flow (EIF) whilst the name real viscous flow (RVF) is reserved for the physical flow. The boundary conditions for the EIF are obtained by differencing continuity and momentum equations for the EIF and RVF, ie the 'deficit formulation'.

The transpiration velocity is given exactly by differencing the continuity equation for the RVF and EIF, then integrating the difference across the shear layer, to give

$$v_{iw} = \frac{1}{\rho_{iw}} \frac{d}{dx} \left\{ \rho_{iw} u_{iw} \delta_A^* \right\} \qquad (1)$$

with $\delta_A^* = \frac{1}{\rho_{iw} u_{iw}} \int_0^\delta (\rho_i u_i - \rho u) d\eta$ and x as distance along the surface, where suffices i and w indicate the equivalent inviscid flow and conditions at the surface of the aerofoil respectively.

It should be noted that δ_A^* is not a streamline of the flow, whereas the 'classical' displacement thickness δ_B^*, defined by equating the total mass flow in the EIF and RVF, is a streamline of the flow. Typically the difference between δ_A^* and δ_B^* is 1%, whereas the difference between δ_A^* or δ_B^* and the first order definition of displacement thickness, which does not take account of pressure variation across the shear layer, is larger (4 to 5% say).

By neglecting the small terms from the integrated form of the difference of the normal momentum equation for the EIF and the RVF, a simple numerical approximation for the difference in wall pressure between the EIF and RVF is derived as:

$$\frac{p_{iw} - p_w}{\rho_{iw} u_{iw}^2} = \kappa^* (\theta + \delta_A^*) \qquad (2)$$

where κ^* is the curvature of the displacement surface. Thus the pressure calculated in the EIF has to be corrected before comparison with experimental values.

In the wake similar boundary conditions apply on a convenient line dividing the flows from the upper and lower surfaces of the aerofoil. The displacement effect of the wake is given by a jump, Δv, in the component of velocity normal to the wake and by analogy with equation (1) is given by

$$\Delta v_i = \frac{1}{\rho_{iu}} \frac{d}{dx} \left\{ \rho_{iu} u_{iu} \delta_u^* \right\} + \frac{1}{\rho_{i\ell}} \frac{d}{dx} \left\{ \rho_{i\ell} u_{i\ell} \delta_\ell^* \right\} \qquad (3)$$

where suffix u refers to the side of the wake developing from the suction side of the aerofoil and ℓ refers to the lower side of the wake.

Fig 1 shows the pressure variation through a normal section of the wake: the pressure variation in the EIF and the RVF are different. The flows outside the wake are made the same by placing a vortex sheet on the dividing streamline in the EIF. By analogy with equation (2) the pressure difference across the vortex sheet is given by:

$$\Delta p_i \equiv p_{iu} - p_{i\ell}$$
$$= \kappa_u^* \rho_{iu} u_{iu}^2 (\delta_u^* + \theta) + \kappa_\ell^* \rho_{i\ell} u_{i\ell}^2 (\delta_\ell^* + \theta_\ell) \quad (4)$$

where $\kappa_u^* = \kappa_{wk} + \frac{d^2\delta_u^*}{dx^2}$ and $\kappa_\ell^* = \kappa_{wk} - \frac{d^2\delta_\ell^*}{dx^2}$

are the curvatures of the upper and lower displacement surfaces (taken as positive if the surface is concave upwards) and κ_{wk} is the curvature of the dividing streamline.

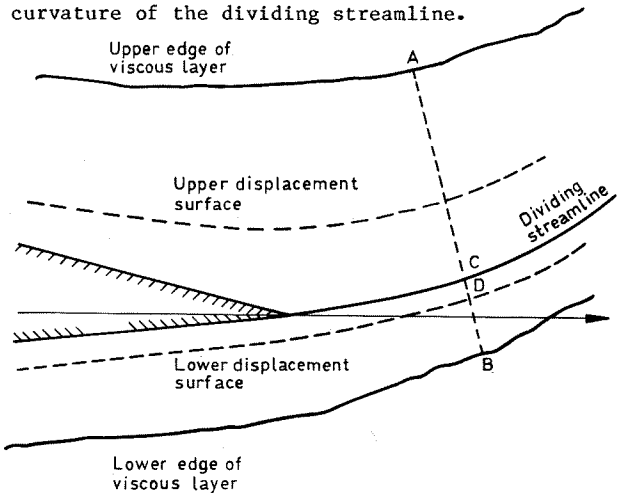

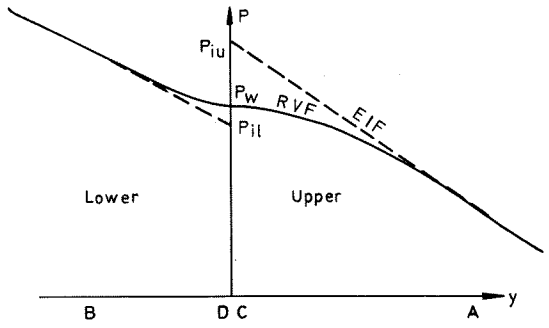

Fig 1

The boundary conditions described above mean that the flow at the trailing-edge is different in the RVF and the EIF. Practical experience tells us that in the RVF the pressures on the upper and lower surface of the aerofoil approach a common value at the trailing edge. However in the EIF equation (2) indicates that there is a jump in pressure at the trailing edge which is given by

$$(\Delta p_i)_{TE} = \left[\kappa_u^* \rho_{iu} u_{iu}^2 (\delta_u^* + \theta_u) + \right.$$
$$\left. + \kappa_\ell^* \rho_{i\ell} u_{i\ell}^2 (\delta_\ell^* + \theta_\ell)\right]_{TE} \quad (5)$$

which is exactly the same value that would be obtained from equation (3) and approaching the trailing edge from upstream. Equation (5) is taken as an expression of the 'Kutta' condition for the EIF and it expresses the continuity of vorticity through the trailing edge region. In a surface-singularity method the 'Kutta' condition can be explicitly satisfied by equating the bound vorticity at the trailing edge of the aerofoil with the vorticity in the wake: for inviscid flow the bound vorticity is set to zero at the trailing edge and all points on the dividing streamline downstream of the trailing edge.

III. Outer Calculation: Inviscid Flow

Although the matching scheme will allow solutions of the Euler equations to represent the outer flow, for simplicity in this paper the outer flow is assumed to be incompressible and irrotational and is given by a solution of Laplace's equation. The outer-flow problem is now linear and a solution of the equivalent inviscid flow is obtained without iteration. Through Green's third identity the solution of Laplace's equation can be expressed as a combination of fundamental solutions distributed on the surface of the aerofoil. In two dimensions the fundamental solutions are taken as sources and vortices and this forms the basis of panel methods. Some of the strengths of the sources and vortices must be specified a priori whilst the remainder are determined by satisfying a proper set of boundary conditions. In a panel method the aerofoil is approximated by an inscribed polygon with N sides and the singularity distributions are approximated by piecewise continuous functions defined on the panels sides of the polygon). In practice the particular mix of sources and vortices, their degree of approximation and the choice of appropriate boundary conditions effect the stability and accuracy of the resultant method.

A numerically stable scheme, developed by Newling[12], is produced if the source distribution is specified as constant on each panel and the vorticity is allowed to varying linearly. The particular mix of sources and vortices is chosen so that the source and vortex density on opposite panels on the upper and lower surface are taken as equal. This reduces the number of unknowns to N + 1 of which N are determined by satisfying a Neumann boundary condition at the centre of each panel of zero normal velocity for inviscid flow and non-zero normal velocity given by equation (1) for the EIF. The final unknown is obtained from the Kutta condition of smooth flow at the trailing edge and is expressed by setting the vorticity at the trailing edge to zero for inviscid flow or by maintaining continuity of vorticity in the EIF as described in the last section.

The shape of the streamline from the trailing edge is calculated by an iterative process. An initial guess at the shape of the streamline is split into panels and, by sweeping down the wake, each panel is progressively aligned with the local flow direction. In the wake the boundary conditions for the EIF are represented by constant source panels along the dividing streamline for the displacement effect and a linearly varying vorticity distribution for the curvature effects. The strengths of the sources and vortices are derived from equations (3) and (4) respectively.

IV. Inner Calculation: Shear Layer

The direct form of the lag-entrainment method given by Green[4], calculates the development of the boundary layer with first order equations from given initial conditions through a specified pressure distribution. East et al[3] derived an inverse form of the method by deriving a functional relationship between the velocity gradient and the slope of the displacement surface. An inverse solution is found by solving this relationship with the momentum integral equation, the entrainment equation and the lag equation for entrainment. The first order boundary-layer equations of Green[4] were first extended to include higher order terms by Weeks[13] and the full equations are given in Ref 8.

Inverse formulations of the shear layer equations as proposed by East et al[3] can only be integrated if the correlation between the shape factors $H(\delta^*/\theta)$ and $H_1\left((\delta - \delta^*)/\theta\right)$ does not contain a minimum. Unfortunately this excludes separated flows where experimental measurements indicate that dH_1/dH passes through the value zero close to separation. Lock[1] has suggested a rearrangement of the equations for the inverse mode including the higher order terms which removes this restriction. The equations are formulated with the independent variable taken as the source strength $S = \frac{1}{\rho_{iw}u_{iw}}\frac{d}{dx}(\rho_{iw}u_{iw}\delta^*_A)$, which is equivalent to the normalised transpiration velocity, v_{iw}/u_{iw}, rather than the slope of the displacement surface. The full set of rearranged equations are given below.

The streamwise momentum integral equation to second order is used in its original and simpler form.

$$\frac{d\theta}{dx} = \tfrac{1}{2}C_f - (\bar{H} + 2 - M^2)\frac{\theta}{u_{iw}}\frac{du_{iw}}{dx} - \frac{1}{\rho_{iw}u_{iw}^2}\frac{d}{dx}\left\{\rho_{iw}u_{iw}^2 f\theta\right\} \qquad (6)$$

where $f = +\frac{\kappa^*}{2}\frac{(\theta + \delta^*)}{\theta} - 0.072\left\{\frac{\bar{H} - 1}{\bar{H}}\right\}\frac{C_\tau}{C_{\tau_{EQ}}}$

and the equation can be reduced to standard form by defining:

$$\tfrac{1}{2}C_f^* = \tfrac{1}{2}C_f - \frac{1}{\rho_{iw}u_{iw}^2}\frac{d}{dx}\left\{\rho_{iw}u_{iw}^2 f\theta\right\} .$$

Some third order terms have been omitted from the full equation and some assumptions have been made about the velocity profile, but full details can be found in Lock and Firmin[1]. The first component of f represents corrections due to the effects of curvature of the mean flow, whilst the second component quantifies the effects of Reynolds normal stresses. It should also be noted that in the direct mode the development of the boundary layer should be calculated through the pressure gradient from the EIF whilst in the inverse mode the pressure gradient in the EIF will be found.

The rearranged form of the relationship between the velocity gradient and the source strength is

$$(H + 1)D\frac{\theta}{u_{iw}}\frac{du_{iw}}{dx} = \frac{dH_1}{d\bar{H}}S + \tfrac{1}{2}C_f^*\left\{\left(1 + \tfrac{1}{5}M^2\right)H_1 - \bar{H}\frac{dH_1}{d\bar{H}}\right\} - C_E\left(1 + \tfrac{1}{5}M^2\right) , \qquad (7)$$

where $D = H_1 - \bar{H}\frac{dH_1}{d\bar{H}} + \frac{1}{5}M^2\left(H_1 + 2\frac{dH_1}{d\bar{H}}\right)$.

The rearranged entrainment equation is

$$D\theta\frac{d\bar{H}}{dx} = H_1 S - \tfrac{1}{5}M^2 H_1 C_f^* - C_E\left(H - \tfrac{2}{5}M^2\right) \qquad (8)$$

and equations (6), (7) and (8) are integrated simultaneously with the lag equation for the entrainment given by

$$\theta\frac{dC_E}{dx} = F\left(C_E, C_{f_0}\right)\left[\frac{2.8}{\bar{H} + H_1}\left\{(C_\tau)_{EQ_0}^{\frac{1}{2}} - \lambda C_\tau^{\frac{1}{2}}\right\} + \left(\frac{\theta}{u_{iw}}\frac{du_{iw}}{dx}\right)_{EQ} - \frac{\theta}{u_{iw}}\frac{du_{iw}}{dx}\left\{1 + 0.075M^2\frac{(1 + 0.2M^2)}{(1 + 0.1M^2)}\right\}\right] \qquad (9)$$

As described in Ref 4 extraneous influences on the turbulence structure are embodied in the coefficient λ in the lag equation (9) and the most important influence in this context is the effect of longitudinal curvature on turbulence structure. To take account of this effect λ is set to $1 + \beta_R\left(1 + \frac{M^2}{5}\right)Ri$ where Ri is the 'Richardson number' and an average value through an equilibrium boundary layer is given approximately by

$$Ri = \frac{2}{3}\frac{\theta}{R}(H + H_1)\left\{\frac{H_1}{\bar{H}} + 0.3\right\} \qquad (10)$$

and β_R is taken from Ref 4 as 7 on a convex wall and 4.5 on a concave wall and R is radius of longitudinal curvature.

The method is completed by the specification of a correlation between $\bar{H}$ and H_1 which can be derived from the velocity profile. Previous correlations were derived from a velocity profile described by 'Coles' wake function

$$\frac{u}{u_e} = 1 - P\left(1 + \cos\frac{\pi y}{\delta}\right) \qquad (11)$$

where δ is the thickness of the layer and in the limit of infinite Reynolds number the inner logarithmic law has collapsed to a slip velocity of $1 - 2P$ at the inner edge of the layer. The $(\bar{H} \sim H_1)$ relationship is illustrated in Fig 2 by curve 1. In practice Green[14] found this $\bar{H} \sim H_1$

relationship to be unsatisfactory and he artificially distorted the curve to give a better account of the development of a boundary layer in zero pressure gradient (see curve 2 in Fig 2). In Ref 4 Green further modified the curve to reproduce the development of attached boundary layers in strongly adverse pressure gradients (curve 3 in Fig 2). Rather than modify the $\bar{H} \sim H_1$ curve it now appears preferable to extend the description of the velocity profile to include these flows and separated flow so that a truly universal $\bar{H} \sim H_1$ correlation can be derived. The two parameter velocity-profile family of Lock provides a major step in this direction.

The velocity profile is assumed to take the form

$$\frac{u}{u_e} = 1 + C_1 \log \eta - C_2 F(\eta) \qquad (12)$$

where $\eta = y/\delta$ and $F(\eta)$ takes the form

$$F(\eta) = 1 \quad \text{if} \quad 0 \leq \eta \leq \eta^* \qquad (13a)$$

$$F(\eta) = f\left\{\frac{\eta - \eta^*}{1 - \eta^*}\right\} \quad \text{if} \quad \eta^* \leq \eta \leq 1 \qquad (13b)$$

and η^* is zero for attached flows and defined empirically for separated flows. Lock[6] found that a close fit to experimental profiles is obtained if f is taken as Coles' wake function, so that

$$f(\xi) = \tfrac{1}{2}(1 + \cos \pi\xi) \qquad (14)$$

where $\xi = \dfrac{\eta - \eta^*}{1 - \eta^*}$.

For the empirical definition of η^* Le Balleur[5] suggested that it should be taken as a function of $\alpha(= \delta^*/\delta)$ and that as α approaches 1 (ie H approaches infinity) then

$$\eta^* \propto 2.3\alpha \ . \qquad (15)$$

Lock proposed a quadratic fairing of the linear relationship implied in equation (15) to the zero value of η^* for attached flow.

The value of $\alpha(= \delta^*/\delta)$ is determined directly by integrating the velocity profile to give

$$\alpha = C_1 + C_2 I_1(\eta^*) \qquad (16)$$

where $I_1(\eta^*) = \eta^* + (1 - \eta^*) \int_0^1 f(\xi) d\xi$.

By matching the velocity profile in equation (13) to the law of the wall as η approaches zero, Lock obtained C_1 in terms of α and the Reynolds number based on the displacement thickness and an equation connecting C_1 and C_f . For given values of α and Re_δ , a Newton iteration was used to determine C_1 from its relationship with α and Re_δ . The skin friction is then determined from the second equation and C_2 follows from equation (16). The velocity profile is then fully determined and H can be determined by integration.

The value of H_1 follows from its definition since

$$H_1 = \frac{\delta - \delta^*}{\theta} = H\left\{\frac{1}{\alpha} - 1\right\} . \qquad (17)$$

The (H, H_1) relationship for $Re_{\delta^*} = 10^5$ is plotted in Fig 2 as curve 4.

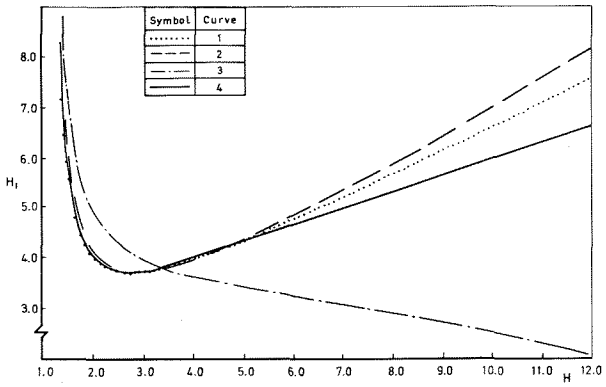

Fig 2

For attached flows the (H, H_1) curve depends upon the Reynolds number and pressure gradient but for separated the curve is almost independent of these parameters. Since we are concerned primarily with separated flows the variation of the (H, H_1) curve with these parameters is not included.

V. Viscous-Inviscid Matching and Stability Analysis

The inviscid and viscous calculations can be matched by taking combinations of the direct and inverse methods of calculating the inviscid flow and the development of the boundary layer. Three popular schemes are indicated in Fig 3, the direct method, the fully inverse method and the semi-inverse method. For flow involving separation of the boundary layer the direct method need not be considered since it involves a direct calculation of the boundary layer through the singularity at separation. In the inverse calculation of the boundary layer an estimate of the normalised transpiration velocity gives an estimate of the velocity u_{iw}^V in the equivalent inviscid flow. The inverse boundary-layer calculation can either be coupled with an inverse inviscid method to give a fully inverse method or with a direct inviscid method to give a semi-inverse method. In the fully inverse method the inverse inviscid method with u_{iw}^V as boundary condition gives a new value of the normalised transpiration velocity and the cycle of calculation is repeated. In the semi-inverse method the normalised transpiration, which was used in the inverse boundary-layer calculation, is also used as boundary conditions in the direct inviscid method to yield another estimate, u_{iw}^I , of the velocity in the EIF. The difference between the two estimates of the velocity in the EIF, $u_{iw}^V - u_{iw}^I$, is used to correct the normalised transpiration velocity and the two simultaneous calculations are repeated.

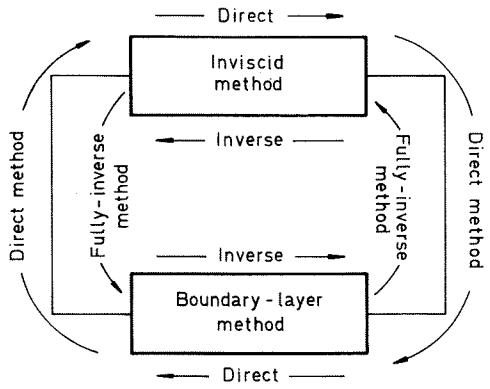

a Direct and fully-inverse methods

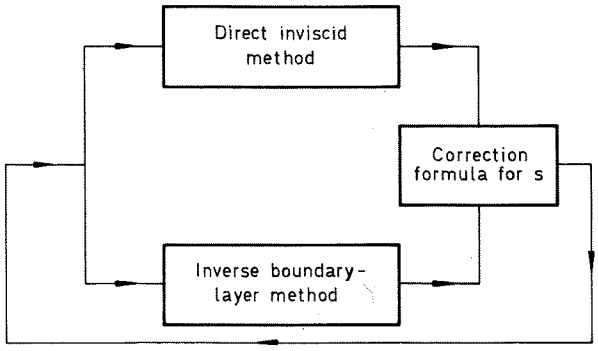

b Semi-inverse method

Fig 3

The converged solution of the matching problem can be characterised by the normalised transpiration velocity and the velocity distribution. The stability of the various schemes (direct, fully inverse and semi-inverse) is studied by examining the behaviour of small perturbations s and u of the converged values of the normalised transpiration velocity S and the velocity U in the inviscid flow and the boundary layer flow. The small perturbations are represented by Fourier expansions and the conditions, under which a particular pair of methods is stable, are determined. The analysis follows the original work of Le Balleur[5] as extended by Lock[6] and Wigton and Holt[9].

Firstly examining the inviscid flow, the normalised transpiration velocity S and velocity U almost coincide with the flow directions normal to and along the wall, thus a perturbation potential ϕ can be defined by $u = U\phi_x$ and $s = \phi_y$. For subsonic flow

$$(1 - M^2)\phi_{xx} + \phi_{yy} = 0 \qquad (18)$$

with boundary conditions $\phi_y = s$ at $y = 0$ and uniform flow at infinity and where M is the local Mach number.

The solution of equation (18) subject to the boundary conditions is

$$\phi = Ce^{i\nu x_e - \beta\nu y}$$

where C is a constant, β is $\sqrt{1 - M^2}$ and the solution involving $e^{+\beta\nu y}$ is discarded as it does not give uniform flow at infinity. On the surface of the aerofoil the perturbations in the velocity and source strength are given by $u(x,0) = Ui\nu\phi(x,0)$ and $s(x,0) = -\beta\nu\phi(x,0)$ thus

$$u(x,0) = -\frac{iU}{\beta} s(x,0) \qquad (19a)$$

or

$$\frac{du}{dx}(x,0) = \frac{U\nu}{\beta} s(x,0) \qquad (19b)$$

which gives the relationship between the perturbations s and u for the direct and inverse inviscid calculations.

For the boundary-layer equations a relationship between the normalised transpiration velocity and the velocity gradient is given by equation (7) so that in the direct mode

$$S = -B\frac{\theta}{U}\frac{dU}{dsc} + C \quad . \qquad (20)$$

For the direct mode a small perturbation in the velocity gradient produces a change in the source strength given by

$$s = -\frac{B\theta}{U}\frac{du}{dx} \qquad (21a)$$

whilst in the inverse mode the response of the boundary layer to a small change in the normalised transpiration velocity is given by

$$\frac{du}{dx} = -\frac{U}{\theta}\frac{s}{B} \qquad (21b)$$

Stability Analysis

If the converged solutions for the velocity and normalised transpiration velocity are U and S then at the nth iteration of any matching scheme let $S^{(n)}$ and $U^{(n)}$ be the current value of the normalised transpiration velocity and velocity. In general different values for these variables are obtained from the inviscid and boundary layer calculations and these are denoted by the superscripts I and V respectively. If the errors in the normalised transpiration velocity at the nth iteration is denoted by $s^{(n)}$, then for the inviscid calculation equation (19b) can be rewritten as

$$\frac{1}{U}\frac{dU}{dx} - \frac{1}{U^{I(n)}}\frac{dU^{I(n)}}{dx} = \frac{\nu}{\beta} s^{I(n)} \qquad (22)$$

and for the boundary layer calculation equation (21b) becomes

$$\frac{1}{U}\frac{dU}{dx} - \frac{1}{U^{V(n)}}\frac{dU^{V(n)}}{dx} = -\frac{1}{\theta B} s^{V(n)} \quad . \qquad (23)$$

Eliminating the velocity U gives

$$\frac{1}{U^{V(n)}}\frac{du^{V(n)}}{dx} - \frac{1}{U^{I(n)}}\frac{dU^{I(n)}}{dx} = \frac{\nu}{\beta} s^{I(n)} + \frac{1}{\theta\beta} s^{V(n)} \quad . \qquad .....(24)$$

This general result is simplified for each of the methods since either the normalised transpiration velocity or the velocity can be equated for the inviscid and boundary layer calculations.

For the direct method the inviscid velocity is used to calculate the development of the boundary layer, ie $U^{I(n)} = U^{V(n)}$ and the general equation reduces to

$$s^{V(n)} = -\frac{\theta B\nu}{\beta} s^{I(n)} .$$

The normalised transpiration velocity resulting from the boundary-layer calculation becomes the estimate for the inviscid calculation at the next iteration, so

$$s^{I(n+1)} = -\frac{\theta B\nu}{\beta} s^{I(n)} \qquad (25)$$

where $-\theta B\nu/\beta$ is an amplification factor and the method converges if $\left|\frac{\theta B\nu}{\beta}\right| < 1$.

For the fully inverse method again the same velocities are used in the inviscid and boundary layer calculations, but now the normalised transpiration velocity resulting from the inverse inviscid calculation is used in the next iteration for the boundary layer calculation and the general equation reduces to

$$s^{V(n+1)} = -\frac{\beta}{\nu\theta B} s^{V(n)} . \qquad (26)$$

The fully inverse method converges if $\frac{\beta}{\nu\theta\beta} < 1$ and the amplification factor is the recriprocal of the value for the direct method.

For the semi-inverse method the same normalised transpiration velocity is used for the inviscid and boundary layer calculations and the general equation reduces to the correction formula first given by Le Balleur[5]

$$s^{(n)} \equiv S - S^{(n)} = \frac{\beta B\theta}{B\theta\nu + \beta} \frac{1}{U^V}\frac{dU^V}{dx} - \frac{1}{U^I}\frac{dU^I}{dx} \qquad (27)$$

where $\frac{\beta B\theta}{B\theta\nu + \beta}$ can be considered as a relaxation factor.

If the typical length of a panel in the inviscid calculation is Δx then the highest frequency contained in the Fourier approximation is $\pi/\Delta x$. The amplification factor for the direct method can be rewritten in terms of the local discretisation and convergence is then obtained if

$$\left|\frac{B\theta\pi}{\beta\Delta x}\right| < 1 . \qquad (28)$$

The amplification factor also depends upon the local state of the boundary layer as described by B and θ . For separating flows B is large and Δx is decreased to improve the accuracy of the integration of boundary-layer equations: the amplification factor becomes greater than unity and the direct method diverges.

For the fully inverse method the amplification factor is the inverse of the factor for the direct method. In general the method converges for separated flows. However the stability of the method depends upon the lowest frequency in the Fourier representation and the amplification factor increases as the computational domain is extended.

For the semi-inverse method the relaxation factor also depends upon the state of the boundary layer and the discretisation in the inviscid method. The relaxation factor varies throughout the field of calculation but is calculated rather than estimated.

If the error $s^{(n)}$ contains only one Fourier mode then the semi-inverse scheme given in equation (27) produces the converged solution, S , in one iteration. In practice the error has many modes and following Wigton and Holt[9] the performance of the relaxation scheme is studied for Fourier modes ν_1 , which are not equal to ν , the frequency used to determine the relaxation factor. From equation (19) the error term $(S - S^{(n)})$ has the form

$$s_1^{(n)} = -\beta\nu_1 C e^{i\nu_1 x} . \qquad (29)$$

From equation (27) the corresponding difference in the velocity gradient parameter is given by

$$\frac{1}{U^V}\frac{dU^V}{dx} - \frac{1}{U^I}\frac{dU^I}{dx} = s_1^{(n)} \frac{(B\theta\nu_1 + \beta)}{\beta B\theta} . \qquad (30)$$

A new approximation to the source strength $S^{(n+1)}$ is given by the relaxation formula as

$$S^{(n+1)} - S^{(n)} = \frac{\beta B\theta}{B\theta\nu + \beta}\left\{\frac{1}{U^V}\frac{dU^V}{dx} - \frac{1}{U^I}\frac{dU^I}{dx}\right\} . \qquad (31)$$

The difference in the velocity parameters are eliminated from equations (30) and (31), and using $S^{(n)} = S - s_1^{(n)}$ gives

$$S^{n+1} = S + \left\{\frac{B\theta\nu_1 + \beta}{B\theta\nu + \beta} - 1\right\} s_1^{(n)} . \qquad (32)$$

The amplification factor for the error mode of frequency ν_1 is given by

$$\mu(\nu_1) = \frac{s_1^{(n+1)}}{s_1^{(n)}} = \frac{S - S^{(n+1)}}{s_1^{(n)}}$$

ie $$\mu(\nu_1) = \frac{\nu - \nu_1}{\nu + (\beta/B\theta)} . \qquad (33)$$

The variation of B^{-1} with $\bar{H}$ for the two-parameter velocity-profile family is shown in Fig 4; B^{-1} is positive for attached flows ($\bar{H} < 2.85$) and negative for separated flows. The change in sign of B^{-1} occurs at $dH_1/dH = 0$, the minimum of H_1 . If ν is chosen to take its maximum value, ν_{max} , then for attached flow $B^{-1} > 0$ and $|\mu(\nu_1)| < 1$ and the method converges. For large values of ν_1 the amplification factor is almost zero leading to fast convergence. For low frequencies the amplification factor is much larger and the convergence rate is correspondingly slower. For separated flow $B < 0$ and if ν is given its maximum value then the method converges for errors made up of high frequency components but for the low frequency components the amplification factor can be greater than unity and the method would

diverge. If the value of ν is allowed to vary from iteration to iteration, then a sequence of ν (with the related relaxation factors) can be selected so that for a part of the sequence of iterations the amplification factor is much less than unity for each component of the error. Numerical experimentation has indicated that a sequence of four relaxation parameters based on an arithmic progression of Fourier frequencies decreasing from the maximum gives the best results.

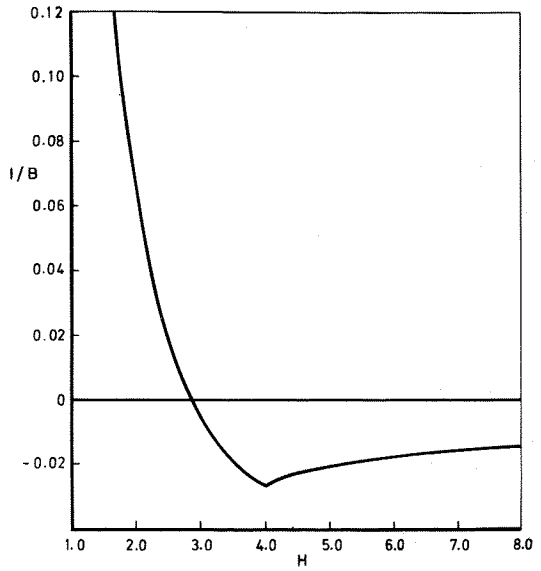

Fig 4

Details of Semi-Inverse Method

Details of the implementation of the semi-inverse method are described. The method must be given the aerofoil coordinates, the Reynolds number, Mach number and angle of incidence. Then the laminar portion of the boundary layer is calculated by a compressible version of the method due to Thwaites[15]. The computer program allows for three different mechanisms for transition to a turbulent boundary layer. Natural transition is predicted by Granville's correlation[16]. If the laminar boundary layer separates before natural transition has been predicted then the development of the laminar separation bubble is calculated by Horton's semi-empirical method[17]. The transition to a turbulent boundary layer can also be fixed at a specified point as long as neither of the other criterion has been satisfied upstream. The development of the turbulent boundary and wake are calculated by the inverse formulation of Green's lag-entrainment method. Although the momentum integral equation given in equation (6) contains all the significant second order terms, not all these terms have been included in the calculations reported in the next section. In particular the correlation for the Reynolds stress terms was derived from attached flow data and there is experimental evidence that the normal stress is significantly larger in separated flows. However there are insufficient data to form a reliable correlation so this term has been omitted from the calculation. In a separated boundary layer it is found experimentally that the growth of the displacement surface is almost linear, thus the terms involving the curvature of the displacement surface have also been ignored.

VI. Comparison with Experimental Results

Detailed measurements of the separated flow on a NACA 4412 have been taken by Wadcock[11] and Hastings[10] at two different Reynolds number and these results are used to show that the semi-inverse method predicts the stall and post-stall behaviour of the aerofoil. The convergence of the matching procedure is studied and it is shown that a sequence of relaxation factors speeds up the rate of convergence.

Wadcock data

The flow about a NACA 4412 aerofoil is calculated at a Reynolds number of 1.52×10^6 and a Mach number of 0.15 in accordance with Wadcock's experiment. The incidence is taken as 13.87°, the geometric incidence measured in the tunnel at which the maximum lift was attained. In the experiment the transition from laminar to turbulent boundary layer is fixed by trips at $x/c = 0.025$ and $x/c = 0.103$ on the upper and lower surfaces respectively: no laminar separation bubbles were detected ahead of the trips. However in the calculation the laminar boundary layer on the upper surface separates at $x/c = 0.012$. The development of the laminar separation bubble is calculated by Horton's semi-empirical method and the shear layer reattaches at $x/c = 0.020$. Thus in the calculation the boundary layer on the upper surface is turbulent before it reaches the trip; some allowance is made for the presence of the trip by increasing the momentum thickness of the boundary layer at the trip by 50%. The size of the increase is chosen so that the predicted momentum thickness agrees roughly with the value at the first measuring station in the experiment at $x/c = 0.62$. The calculation of the boundary includes the effect of longitudinal curvature on turbulence structure, but no other second order effects. The representation of the EIF includes the effect of wake thickness but not wake curvature.

The initial guess for the strength of the source distribution linking the inviscid and viscous flows is taken as 0.0028 which corresponds to the growth of a boundary layer in zero pressure gradient. The initial guess for the strength of the source distribution does not have to be close to the final solution to obtain convergence, thus solutions can be obtained at any incidence without having to use the converged solution from a slightly lower incidence as an initial guess. As described in section V the relaxation parameters in the iterative solution are defined locally in the field depending upon the panel size and the state of the boundary layer. In Fig 5 it can be seen that the rate of convergence is slow if the relaxation parameters are based on the local panel size as implied by equation (33). However a sequence of relaxation parameters produces more rapid convergence. For each sequence of relaxation parameters, the first two iterations have a relaxation parameter based on the panel length. In subsequent iterations an arithmetic progression of panel lengths is used to define the relaxation parameter, ie the third iteration uses twice the panel length, the fourth iteration three times the panel length, etc.

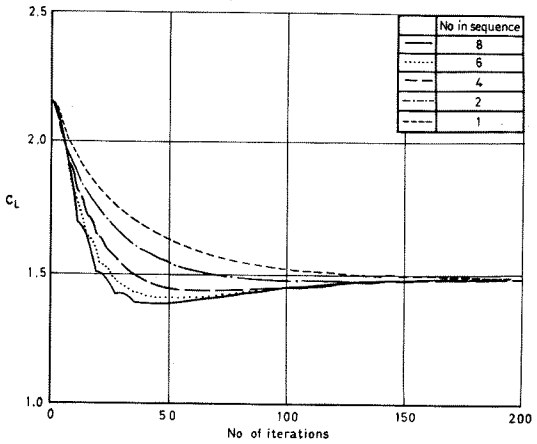

Fig 5

After the specified number in the sequence has been reached the next iteration uses the panel length and the process is repeated. The cyclic nature of this process can be seen for the first thirty iterations with eight parameters in the sequence in Fig 5: relaxation parameters based on small multiples of the panel length result in a small decrease in lift whilst parameters based on large multiples of the panel length produced large reductions in lift.

The best results are obtained with between two and four relaxation parameters in the sequence: a smaller number produces an initially slower rate of convergence whilst a larger number soon over-predicts the loss of lift and the solution is slow to recover. The location on the upper surface of the point of intermittent separation of the boundary layer at which H is approximately 2.7 as the iterations progress is shown in Fig 6. For a sequence containing eight relaxation parameters the long wavelength errors are damped as well as the short wavelength errors and the theoretical separation point quickly moves to the region in which separation occurs in the experiment. The more rapid forward movement of the separation point with increasing number of relaxation parameters in the sequence explains the variation of lift coefficient shown in Fig 5.

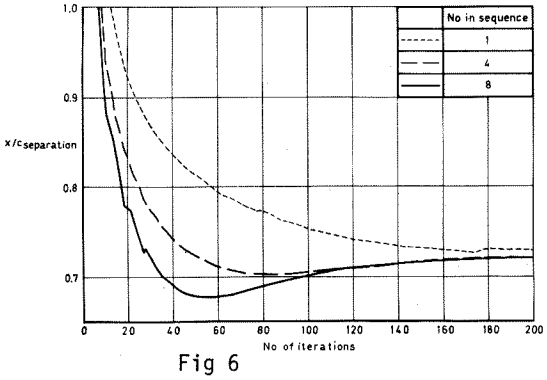

Fig 6

The data published by Wadcock include no allowance for tunnel constraint, but more importantly the tunnel reference velocity is measured at a point influenced by the velocity field of the aerofoil. The experimental set-up used by Wadcock is shown in Fig 7. The model is placed in a two-dimensional insert in a 10ft (3.048M) circular wind tunnel. The reference

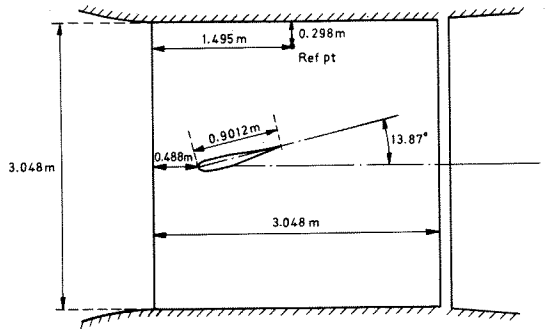

Fig 7

velocity was measured at a point about 1 chord from the pressure side of the aerofoil in line with the trailing edge and this reference velocity was used to non-dimensionalise the pressure and lift. The error induced by using this reference velocity is assessed by calculating the inviscid flow about the aerofoil and its image system representing the effects of the tunnel walls. According to Ref 18 a circular tunnel can be represented approximately by a rectangular tunnel with a height given by 84.3% of the diameter of the circular tunnel. The inviscid flow about the aerofoil and its image system in the equivalent rectangular tunnel are calculated by the surface-singularity method of Hess and Smith[19] with the aerofoil at incidences of 4° and 13.87°. From these values it is deduced that an incidence of 9.3° will give a lift coefficient of 1.669 (the value given by Wadcock at an angle of incidence of 13.87° in the experiment). At an angle of incidence of 9.3° the velocity at the reference point is only 90.6% of the freestream value which implies that all the quoted velocities can be in error by up to 10%.

The classical constraint corrections, calculated by the method of Ref 18 are not very large. Solid and wake blockage imply an increase in velocity of 1.14% whilst the constraint correction gives an increase in incidence of 0.278° and a decrease in lift coefficient of 0.0422.

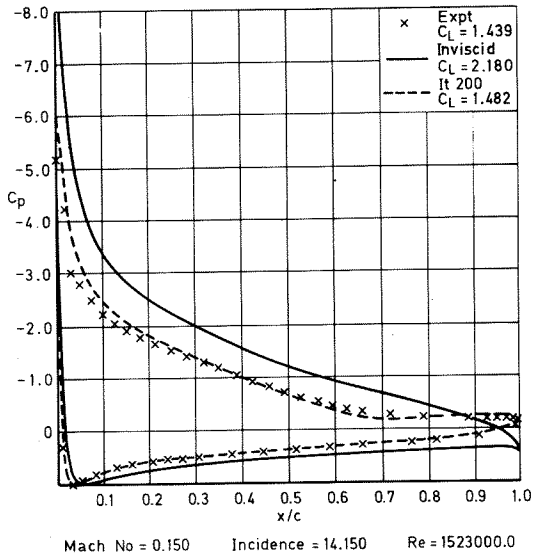

Fig 8

These corrections are taken into account by calculating the flow about the NACA 4412 aerofoil at an incidence of 14.15°. The inviscid and converged viscous pressure distributions are given in Fig 8. These are compared with the experimental pressure distribution which has been corrected for an 8% error in the reference velocity.

In spite of the rather uncertain nature of the corrected experimental data and the lack of second order effects in the theoretical calculation there is reasonable agreement between the measured and calculated pressure distributions. However a more detailed examination of the development of the boundary layer on the upper surface indicates the need to include some second order effects. In Fig 9 it can be seen that there is good agreement with the measured shape parameter at x/c = 0.62, but the theoretical method predicts full separation (ie H = 4.0) at x/c = 0.745 which is upstream of the measured position at x/c = 0.87. After separation the rate of growth of H is too large and this could be caused by the omission of second order effects, in particular normal stress.

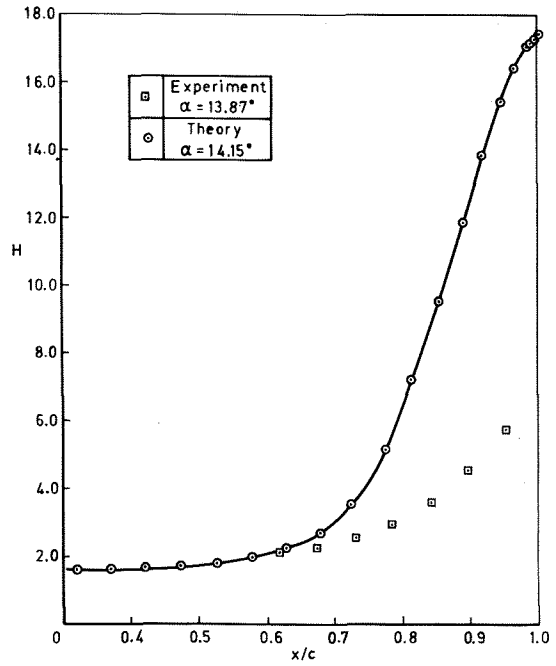

Fig 9

The comparison demonstrates that the matching procedure produces a converged solution which has all the essential characteristics of separated flow about an aerofoil. The lift coefficient is predicted reasonably well but some second order terms will have to be included in the calculation of the boundary layer before the drag can be estimated adequately.

Hastings' data

A two dimensional model with the NACA 4412 section has also been tested in the RAE 3.962m × 2.743m (13ft × 9ft) atmospheric low-speed wind tunnel during the first quarter and the last quarter of 1982 by Hastings[10]. The chord of the model is 1.0 m and it is mounted horizontally spanning the tunnel. The Reynolds and Mach number of the test are 4.17×10^6 and 0.18 respectively. To avoid the occurrence of laminar separation bubbles the transition from laminar to turbulent boundary layer is fixed by placing a single wire at x/c = 0.014 and 0.113 on the upper and lower surfaces respectively for the tests in the first quarter of 1982. For the tests in the last quarter of 1982 distributed roughness was added ahead of the transition wires. For both tests boundary-layer forces are placed down the chord at 0.85 m on either side of the mid-span to maintain reasonably steady and uniform separated flow over the mid-portion of the wing and these are effective up to an angle of incidence of 13°. The main set of data is taken at an incidence of 12.23° for which the separation point was at about x/c = 0.8. The lift coefficient was calculated by integrating the static pressure distribution around the mid-span of the wing. A laser doppler anemometer was used to obtain mean velocity profiles at eight stations between 0.59 < x/c < 0.99, whilst a pitot probe was used at x/c = 0.2 and 0.4.

The flow about the NACA 4412 aerofoil at 12.23° incidence is calculated with transition from laminar to turbulent boundary layer fixed in accordance with the experimental trips. The theoretical method does not implicitly contain an estimate of the change in the state of the boundary layer as it passes over the trip, but this is simulated by increasing the momentum thickness at the trip in the following manner. The calculated value of the momentum thickness of the laminar boundary layer at x/c = 0.014 (the position of the trip on the upper surface) is 0.000037 m which is to be compared with a trip-wire diameter of 0.0002 m. The momentum thickness of the boundary layer is increased by 0.0002 m at the trip and as indicated in Fig 10 there is reasonable agreement with the momentum thickness measured at x/c = 0.2 and 0.4.

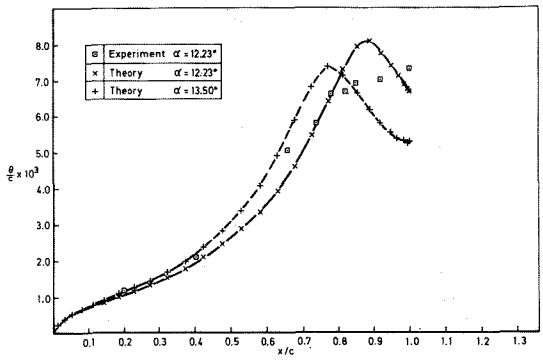

Fig 10

Calculations with the same increase in momentum thickness at the trip are repeated for angles of incidence between 0° and 14.5°: the lift coefficients are compared with the experimental and inviscid values in Fig 11. Up to an incidence of 12.23° there is good agreement with the experimental results. However the theoretical results extend beyond the range of the experimental results and indicate a decrease in the lift coefficient as the separation point moves towards the leading edge.

Also included on Fig 11 are some results using a direct coupling, ie the boundary layer is

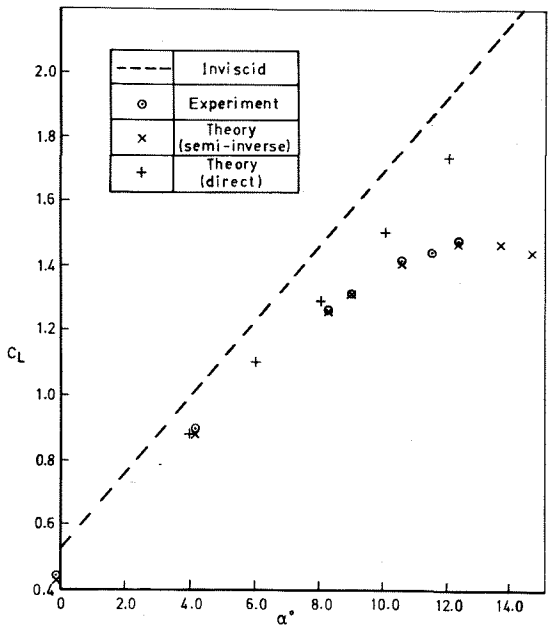

Fig 11

calculated in direct mode up to the point of separation after which an empirical correlation is used to determine the displacement thickness rather than an integration of the boundary layer equations. The direct method predicts that the boundary layer on the upper surface separates at x/c = 0.999 at an angle of incidence of 4°. As the angle of incidence is increased the separation point moves forward very slowly and it has only reached x/c = 0.96 at an angle of incidence of 12°. At an incidence of 14° the values of the lift coefficient predicted in the iterative cycle become very erratic and eventually the boundary-layer calculation fails. The direct method of coupling fails to produce results which agree with the experimental values as soon as there is a significant region of separated flow on the aerofoil.

The calculated and measured pressure distributions are compared in Fig 12 and the two distributions are similar except over the separated region for which the correct shape of the pressure distribution is predicted but at a slightly too high level. Using the criterion that a shape parameter of 4.0 identifies the point of separation, then separation in the experiment occurs just ahead of x/c = 0.80 whilst in the calculation it occurs just ahead of x/c = 0.90 and this accounts for the difference in levels of pressure in the separated region. There are two easily identified factors which could account for the difference in separation position: the change in momentum thickness at the trip could be incorrect or the three-dimensional nature of the flow in the wind tunnel could produce a change in the effective incidence of the model. The plausibility of these factors is checked by performing a calculation with the change in the momentum thickness at the trip increased from 0.0002 to 0.0003 and another calculation at an angle of incidence of 13.5°. Increasing the momentum thickness moves the separation point forward to x/c = 0.82 but the lift coefficient falls to 1.38 which is 7% below

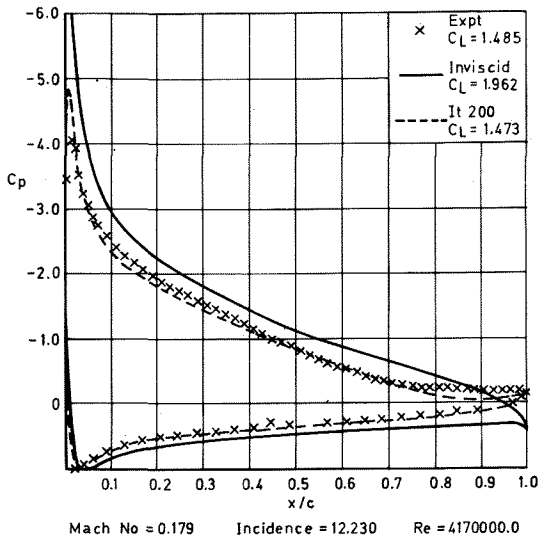

Fig 12

the experimental value. Alternatively the increase in incidence moves the separation point to x/c = 0.79 and increases the lift coefficient slightly to 1.476 which is only 0.6% below the experimental value. Thus calculation at an angle of incidence of 13.5° rather than 12.23° are in closer agreement with the experimental pressure distribution and lift coefficient as shown in Fig 13 which suggests that the three-dimensional nature of the flow in the wind tunnel induces an upwash at the model which increases the effective incidence.

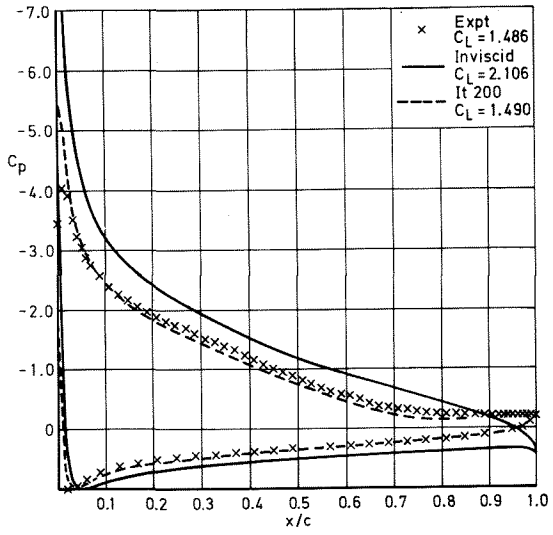

Fig 13

Evaluation of the measurements of the velocity profiles close to and in the separated region by the laser doppler anemometer is at a preliminary stage but it seems worthwhile comparing the available results with the theoretical predictions. The momentum thickness from the experiment and the calculations at angles of incidence of 12.23° and 13.5° are compared in Fig 10. The measurements by the pitot taken at x/c = 0.2 and 0.4 are closer to the calculation at an incidence of 13.5°. For the remaining measurements by

laser doppler anemometer the same calculations more closely reflect the trend of the measurements. However it should be noted that the measurements of the velocity profile are rather unreliable close to the surface and this portion of the profile makes a major contribution to the momentum deficit. Fig 14 indicates that there is good agreement between the measured displacement thickness and the values calculated for an angle of incidence of 13.5°, although it should be pointed out that the displacement thickness is one order of magnitude larger than the momentum thickness. Reasonable agreement of H is shown in Fig 15 and this would be improved along the momentum thickness in the last 20% of the chord by the inclusion of normal stress terms in the calculation.

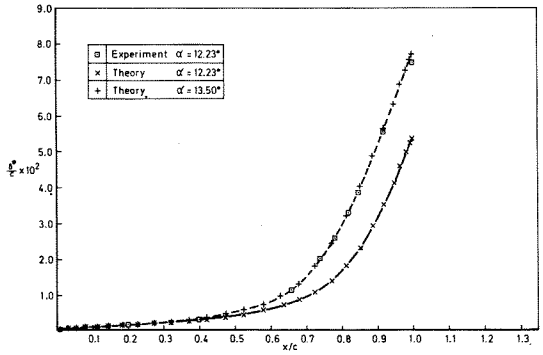

Fig 14

In summary the semi-inverse method adequately predicts the lift for a NACA 4412 section up to and beyond the stall although there are detailed differences in the surface pressure distribution. A detailed comparison of the experimental values at an incidence of 12.23° are in good agreement with a calculation at an incidence of 13.5°: this may arise from a change in the effective incidence of the model induced by three-dimensional features in the flow.

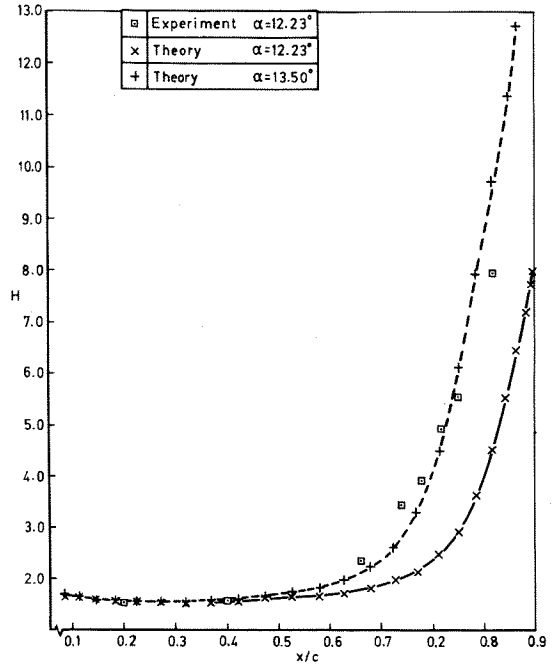

Fig 15

VII. Conclusions

An integral boundary layer method is extended to calculating separated boundary layers by assuming a two parameter description of the velocity profile which adequately describes current measurements of separated profiles. Coupling the boundary layer method with an inviscid flow by a semi-inverse method gives a reasonable estimate of the maximum lift coefficient. A good estimate of the drag for separated flows cannot be made until the boundary layer method includes such second order terms as normal stress. However no universal correlation for normal stress in terms of integral parameters of the boundary layer for separating and separated flows has yet been established.

The stability of various matching schemes, direct, fully-inverse and semi-inverse are studied by a linear stability analysis. This analysis indicates that the semi-inverse method of a direct inviscid calculation coupled with an inverse calculation of the boundary layer is the most suitable choice for a mixture of attached and separated flows in external aerodynamics.

The linear stability analysis of the coupling methods yields optimum relaxation factors which are useful estimates for the non-linear problem. The relaxation factors depend upon the grid size and the local state of the boundary layer and they take different values of points throughout the field of calculation. It is also demonstrated that a systematic variation of the relaxation factor from iteration to iteration leads to a faster rate of convergence.

References

1 Lock, R.C. and Firmin, M.C.P. 'Survey of techniques for estimating viscous effects in external aerodynamics.' Proceedings of IMA Conference on Numerical Methods in Aeronautical Fluid Dynamics, 30 March-1 April 1981, edited by P. Roe, Academic Press (1983).

2 Catherall, D. and Mangler, K.W. 'The integration of the two-dimensional laminar boundary-layer equations past the point of vanishing skin friction.' JFM Vol 26, Pt 1, pp 163-182 (1966).

3 East, L.F., Smith, P.D., Merryman, P.J. 'Prediction of the development of separated turbulent boundary layers by the lag-entrainment method'. RAE Technical Report 77046 (1977).

4 Green, J.E., Weeks, D.J., Brooman, J.W.F. 'Prediction of turbulent boundary layers and wakes in compressible flow by a lag-entrainment method.' RAE Technical Report 72231 (1972).

5 Le Balleur, J.C. 'Strong matching method for computing transonic viscous flows including wakes and separations.' La Recherché Aérospatiale No.1981-3, pp 21-45, English translation.

6 Lock, R.C. 'Private communication'.

7 Mahgoub, H.E.H. and Bradshaw, P. 'Calculation of turbulent-inviscid flow interactions with large normal pressure gradients.' AIAA Journal Vol 17, No.10, pp 1025-29 (1979).

8 East, L.F. 'A representation of second-order bounday-layer effects in the momentum integral equation and in viscous-inviscid interactions.' RAE Technical Report 81002 (1981).

9 Wigton, L.B. and Holt. 'Viscous-inviscid interaction in transonic flow.' AIAA Paper No.81-1003 (1981).

10 Hastings, R.C. 'Private communication'.

11 Wadcock, A.J. 'Flying hot-wire study of two-dimensional turbulent separation on a NACA 4412 airfoil at maximum lift.' PhD thesis, California Institute of Technology (1978).

12 Newling, J.C. 'An improved two-dimensional multi-aerofoil program.' HSA-MAE-R-FDM-0007 (1977).

13 Weeks, D.J. 'RAE unpublished paper'.

14 Green, J.E. 'Application of Head's entrainment method to the prediction of turbulent boundary layers and wakes in compressible flow.' RAE Technical Report 72079 (1972).

15 Thwaites, B. (Ed). 'Incompressible aerodynamics.' Clarendon Press (1960).

16 Granville, P.S. 'The calculation of viscous drag of bodies of revolution.' David Taylor Model Basin, Report 849 (1953).

17 Horton, H.P. 'A semi-empirical theory for the growth and bursting of laminar separation bubbles.' ARC CP 1073 (1967).

18 Garner, H.C., Rogers, E.W.E., Acum, W.E.A., Maskell, E.C. 'Subsonic wind tunnel wall corrections.' AGARDograph 109 (1966).

19 Hess, J.L. and Smith, A.M.O. 'Calculation of potential flow about arbitrary bodies.' Progress in Aeronautical Sciences, Vol 8, pp 1-139, Pergamon Press (1967)